

Article

## An Improved ASTER Index for Remote Sensing of Crop Residue

Guy Serbin <sup>1,\*</sup>, E. Raymond Hunt Jr. <sup>2</sup>, Craig S. T. Daughtry <sup>2</sup>, Gregory W. McCarty <sup>2</sup> and Paul C. Doraiswamy <sup>2</sup>

<sup>1</sup> ASRC Management Services, USDA/FAS Office of Global Analysis, Washington, DC 20250, USA

<sup>2</sup> USDA/ARS Hydrology and Remote Sensing Laboratory, Beltsville, MD 20705, USA;  
E-Mails: raymond.hunt@ars.usda.gov (E.R.H., Jr.); craig.daughtry@ars.usda.gov (C.S.T.D.);  
greg.mccarty@ars.usda.gov (G.W.M.); paul.doraiswamy@ars.usda.gov (P.C.D.)

\* Author to whom correspondence should be addressed: E-Mail: guy.serbin@gmail.com;  
Tel.: +1-202-720-0143; Fax: +1-202-720-1295.

Received: 13 July 2009; in revised form: 30 October 2009 / Accepted: 5 November 2009 /

Published: 11 November 2009

---

**Abstract:** Unlike traditional ground-based methodology, remote sensing allows for the rapid estimation of crop residue cover ( $f_R$ ). While the Cellulose Absorption Index (CAI) is ideal for  $f_R$  estimation, a new index, the Shortwave Infrared Normalized Difference Residue Index (SINDRI), utilizing ASTER bands 6 and 7, is proposed for future multispectral sensors and would be less costly to implement. SINDRI performed almost as well as CAI and better than other indices at five locations in the USA on multiple dates. A minimal upgrade from one broad band to two narrow bands would provide  $f_R$  data for carbon cycle modeling and tillage verification.

**Keywords:** crop residue; non-photosynthetic vegetation; ASTER; agricultural remote sensing

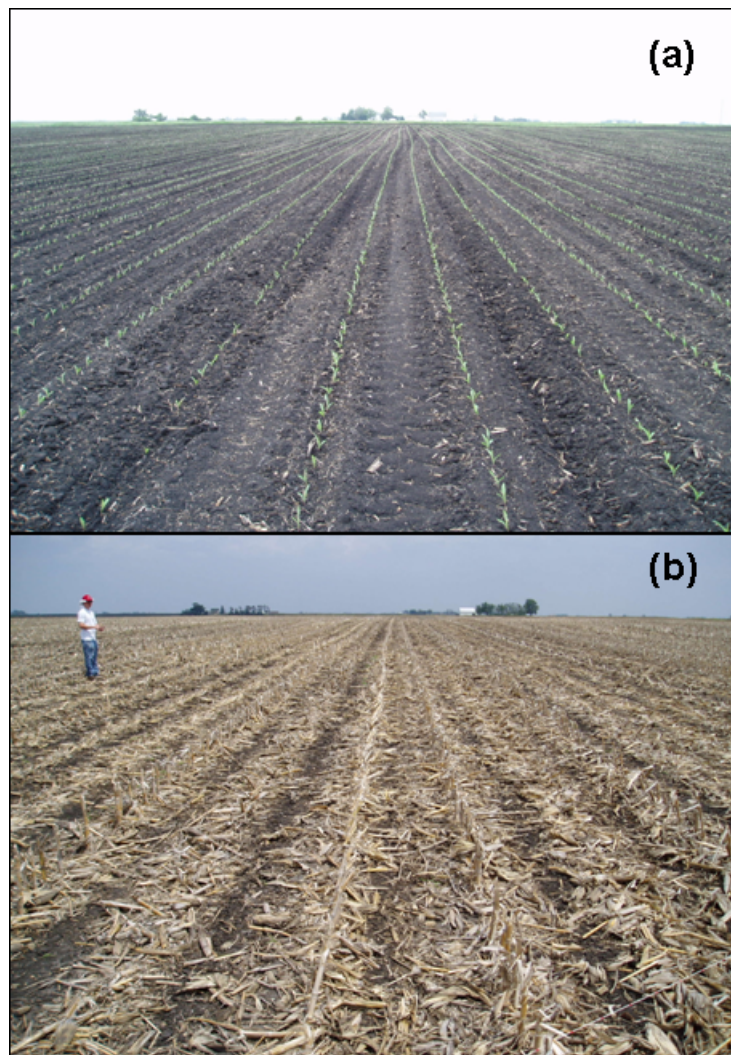
---

### 1. Introduction

Agricultural soils are an important reservoir of carbon globally and are a major component in models of the global carbon cycle [1-4]. One important input into agricultural soil organic carbon (SOC) models is tillage practice. Conventional tillage practices (Figure 1a) greatly disturb the soil surface and plow under crop residues (i.e., non-photosynthetic vegetation), and can result in a decrease in SOC over time [2]. However, reduced- and conservation tillage (Figure 1b), which minimally disturb the soil surface and crop residues, allow for the sequestration of atmospheric carbon to the

soil [2]. Reduced- and conservation tillage methods require fewer passes over the soil with farm machinery, thus saving fuel and further reducing net agricultural greenhouse gas emissions [5,6]. Residues from crops and other vegetation act as a barrier to wind and water, reducing erosion and evaporation. The breakdown of surface residues increases soil fertility over time. Whereas conservation tillage cropping systems often have reduced yields in comparison with conventional-till systems, cost reductions in labor, equipment, fuel, and irrigation increase net farm profitability [5-7], particularly when coupled with conservation subsidies and the sale of carbon sequestration credits [1,2]. Tillage practice is also an important variable for biogeochemical models in agricultural soils [1,2]. Increasing demand for biofuels can result in increased tillage or encourage the harvesting of crop and vegetation residues [8]. These factors all require a more efficient method for measuring and monitoring vegetation residue cover compared to ground surveys.

**Figure 1.** Photographs of (a) conventional (intensive) and (b) conservation (no-till) tillage from the area surrounding Ames, Iowa, USA.



Remote sensing of crop residue cover ( $f_R$ ) offers a rapid means for determination of tillage method when compared with ground-based methods, such as the line-point transect methodology [9-12]. A number of remote sensing indices for discrimination of  $f_R$  have been devised for Landsat Thematic

Mapper (TM) [13-15], the NASA Terra Advanced Spaceborne Thermal Emission and Reflection Radiometer (ASTER) sensor [12], hyperspectral methods [11,12], and spectral angle methods [16]. Serbin *et al.* [17] compared six indices for  $f_R$  estimation for spectral contrast between soils, crop residues, and green vegetation for Landsat TM, ASTER, and hyperspectral shortwave infrared (SWIR) sensors utilizing the soil spectral library of Brown *et al.* [18]. With extensive field and laboratory data, the Landsat TM-based indices fared the worst and the hyperspectral Cellulose Absorption Index (CAI) [11] fared the best [12,17], with the ASTER Lignin-Cellulose Absorption (LCA) index in between. Among the Landsat TM-based indices, the Normalized Difference Tillage Index (NDTI) [14] performed the best [17].

While CAI may be the best index for  $f_R$ , it is currently impractical to use as it can be only acquired from space using the EO-1 Hyperion sensor, which is past its designed lifetime, suffers from detector scan-line problems and noise, and has a narrow (7.5 km) swath width [19]. ASTER has been applied for crop residue and non-photosynthetic vegetation cover mapping in previous studies [12,20-23]. Many ASTER scenes of agricultural areas were collected prior to the shortwave infrared (SWIR) detector failure in April 2008 [24]. The aim of this research is to evaluate a new ASTER-based index, the Shortwave Infrared Normalized Difference Residue Index (SINDRI), which utilizes ASTER SWIR bands 6 and 7, against CAI, LCA, and NDTI. SINDRI, if effective, would allow for the least costly upgrade from Landsat TM Band 7 on future multispectral sensors for detection of vegetation residue, improving the accuracy of soil carbon-cycle models.

## 2. Remote Sensing Crop Residue Cover

### 2.1. Spectral Properties of Soils and Residues

Remote detection of  $f_R$  works best when there is a clear contrast among the index values of  $f_R$  and those of soils and live green vegetation [12,17]. Soil spectral properties are a function of multiple factors, including mineralogy and composition [18,25-29], water content [30-34], grain size [26,27,35], structure [36], and SOC [17,18,34,37,38]. Crop residue and soil can be very similar spectrally below 1,920 nm (Figure 2), as shown by Daughtry *et al.* [12], except for an absorption feature around 1,440 nm shared with vegetation and atmospheric water vapor [39,40]. However, above 1,920 nm the O-H bending and C-O stretching combination at 2,101 nm exists for cellulose and other sugars [12,26,40-42], which is not found in common soil minerals [43], and provides a clear contrast between soils and crop residues [17].

### 2.2. Previously Existing Spectral Indices for Crop Residue Detection

Within this study, three established spectral indices were used for estimation of  $f_R$ . The first index, CAI [11], utilizes three narrow spectral bands:

$$CAI = 100 \cdot \left( \frac{R_{2031} + R_{2211}}{2} - R_{2101} \right) \quad (1)$$

where  $R$  denotes reflectance and the subscripts denote 11 nm-wide bands centered at 2,031, 2,101, and 2,211 nm wavelength. CAI essentially measures the depth or intensity of the 2,101 nm absorption [40,41] as shown in Figure 2.  $R_{2031}$  is determined at 2,031 nm wavelength and not 2,000 nm in order to avoid a narrow atmospheric CO<sub>2</sub> absorption feature centered at 2,010 nm [39,44].

**Figure 2.** Visible, NIR, and SWIR spectra acquired from a ground-based spectrophotometer of soil, crop residue, and live corn canopy along with ASTER, Landsat TM, and CAI bands. 2031, 2101, and 2211 denote CAI bands. Soil and residue spectra were acquired in the lab, corn canopy outdoors. Relative spectral response functions for ASTER and Landsat TM are courtesy USGS [45]. Abbreviations in legend: Cla is Clarion loam (0.8% SOC) from Ames, IA; CrA, Hm, and Res are Crosier loam (0.5% SOC), Houghton muck (44.9% SOC), and 7 month old corn residue from a field with standing stubble from Fulton, IN, respectively; LC is live corn canopy at silking (R1) [46] stage in Beltsville, MD.

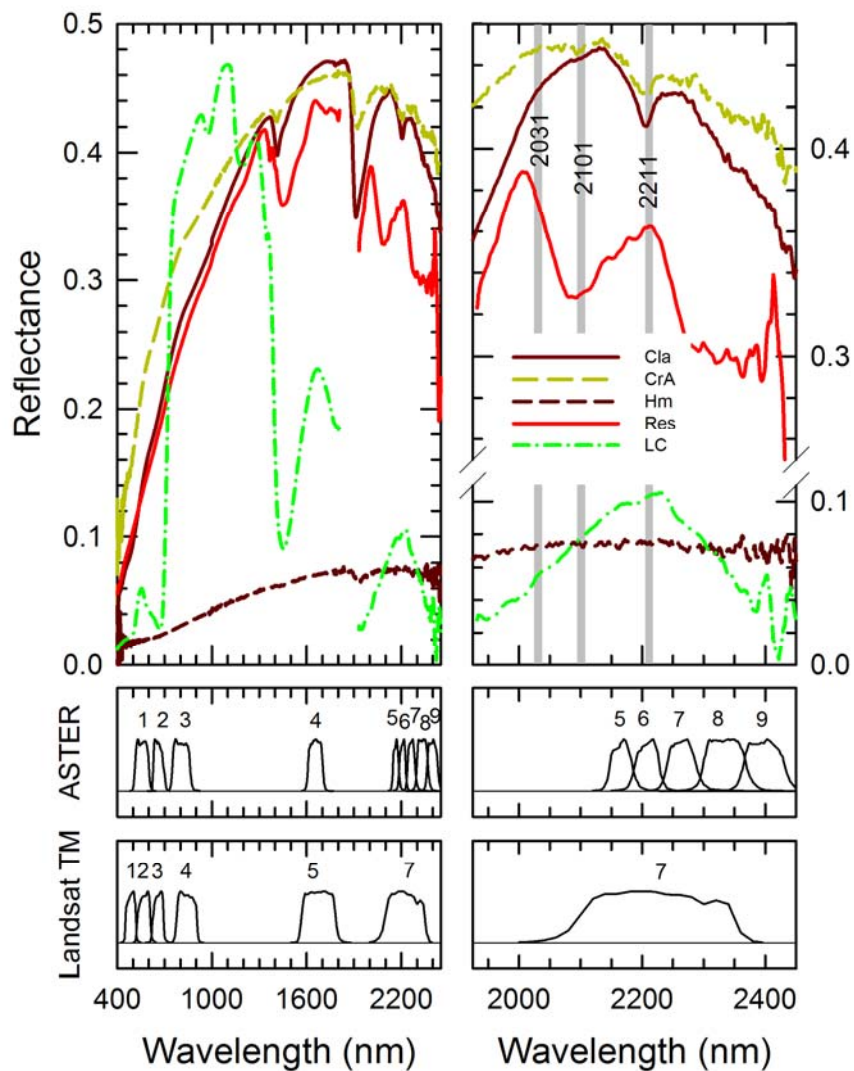


**Table 1.** Dates, locations, sensors, residue and soil water contents, and comparisons of the Cellulose Absorption Index (CAI), the Shortwave Infrared Normalized Difference Residue Index (SINDRI), the Lignin-Cellulose Absorption Index (LCA), and the Normalized Difference Tillage Index (NDTI). *N*, *RMSE*, and *r*<sup>2</sup> denote number of samples, root mean square error, and coefficient of determination, respectively, in comparison between spectral index value and line-point transect ground-truth of crop residue cover. Three-class accuracy assessments (3 × 3 acc.) for 0%–15%, 15%–30%, and 30%–60% residue cover classes for the four indices evaluated in this paper. Classification accuracy is assessed using *k*-hat, an estimate of the kappa statistic, and the Z-statistic (Z-stat), which is used to test the null hypothesis that classification accuracy is not significantly different from chance. Comp. denotes composite (mean) values. Non-ASTER data were acquired using either a ground-based spectroradiometer or an airborne hyperspectral sensor. CMD and PIL denote Centreville, MD and Pesotum, IL, respectively. bna and dna denote “bands not available” and “data not available”, respectively.

Location	Beltsville, MD					CMD 10 Apr 2007 Air- borne	Ames, IA			Fulton, IN		PIL 8 Jun 2006 Air- borne	Composite (mean) value	
	Date	20 May 2002	22 May 2002	10 Jun 2003	1 Jun 2004		2 Jun 2004	22 May 2005	19 May 2007	27 May 2007	29 May 2006			6 Jun 2007
Sensor	Ground					Air- borne	ASTER			Airborne		Air- borne		
<i>N</i>	77	95	41	41	71	32	107	104	104	95	136	37		
Residue Water g g <sup>-1</sup>	0.09	0.08	1.80	1.10	0.10	dna	dna	dna	dna	dna	dna	dna		
Soil Water g g <sup>-1</sup>	dna	0.09	0.30	0.28	0.09	dna	dna	dna	dna	dna	dna	dna		
CAI	<i>r</i> <sup>2</sup>	0.899	0.882	0.935	0.554	0.815	0.885	bna	bna	0.821	0.798	0.829	0.722	<b>0.814</b>
	<i>RMSE</i>	0.097	0.094	0.085	0.151	0.152	0.100	bna	bna	0.078	0.117	0.107	0.128	<b>0.111</b>
	3×3 acc.	0.829	0.779	0.902	0.732	0.761	0.813	bna	bna	0.654	0.674	0.695	0.757	<b>0.759</b>
	<i>k</i> -hat	0.68	0.63	0.84	0.13	0.61	0.66	bna	bna	0.42	0.51	0.45	0.51	<b>0.54</b>
	Z-stat	8.90	9.62	11.82	0.77	8.19	5.81	bna	bna	5.26	6.73	5.43	3.62	<b>6.61</b>
SINDRI	<i>r</i> <sup>2</sup>	0.853	0.811	0.769	0.640	0.835	0.596	0.611	0.605	0.674	0.821	0.834	0.868	<b>0.743</b>
	<i>RMSE</i>	0.117	0.119	0.159	0.135	0.144	0.187	0.106	0.116	0.106	0.093	0.106	0.088	<b>0.123</b>
	3 × 3 acc.	0.855	0.768	0.805	0.780	0.887	0.750	0.710	0.587	0.712	0.653	0.811	0.784	<b>0.758</b>
	<i>k</i> -hat	0.73	0.61	0.69	0.43	0.81	0.53	0.42	0.30	0.51	0.48	0.68	0.57	<b>0.56</b>
	Z-stat	9.93	9.19	7.48	3.22	12.96	4.13	5.56	3.95	6.93	6.39	10.16	4.21	<b>7.01</b>
LCA	<i>r</i> <sup>2</sup>	0.815	0.767	0.634	0.487	0.842	0.651	0.575	0.632	0.664	0.390	0.618	0.860	<b>0.661</b>
	<i>RMSE</i>	0.131	0.132	0.200	0.161	0.140	0.174	0.111	0.112	0.107	0.171	0.161	0.091	<b>0.141</b>
	3 × 3 acc.	0.737	0.737	0.780	0.707	0.789	0.813	0.673	0.606	0.587	0.547	0.611	0.703	<b>0.691</b>
	<i>k</i> -hat	0.51	0.55	0.64	0.09	0.63	0.66	0.34	0.33	0.29	0.34	0.34	0.43	<b>0.43</b>
	Z-stat	6.18	7.87	6.61	0.57	7.71	5.51	4.04	4.11	3.67	4.17	4.22	2.97	<b>4.80</b>
NDTI	<i>r</i> <sup>2</sup>	0.281	0.247	0.089	0.272	0.569	0.229	0.490*	0.640*	0.004	0.419	0.182	0.161	<b>0.299</b>
	<i>RMSE</i>	0.258	0.227	0.316	0.192	0.232	0.259	0.122*	0.111*	0.185	0.167	0.235	0.222	<b>0.210</b>
	3 × 3 acc.	0.618	0.589	0.366	0.780	0.634	0.563	0.720*	0.625*	0.462	0.463	0.589	0.649	<b>0.588</b>
	<i>k</i> -hat	0.16	0.28	0.11	0.32	0.37	0.12	0.44*	0.37*	0.01	0.22	0.24	0.33	<b>0.25</b>
	Z-stat	1.49	3.48	0.73	1.92	4.07	0.76	5.28*	4.94*	0.06	2.61	2.48	1.80	<b>2.47</b>

\* denotes NDTI calculated by averaging ASTER Bands 5-8 into an equivalent Landsat TM band 7.

The second index, LCA [12], is a similarly devised index for the ASTER sensor:

$$LCA = 100 \cdot [2 \text{ ASTER6} - (\text{ASTER5} + \text{ASTER8})] \tag{2}$$

where ASTER5, ASTER6, and ASTER8 denote ASTER shortwave infrared (SWIR) bands 5 (2,145–2,185 nm), 6 (2,185–2,225 nm), and 8 (2,295–2,365 nm) [47]. The last index, NDTI [14], was developed for the Landsat TM platform and was used in this study for comparison between hyperspectral, ASTER, and Landsat sensors:

$$NDTI = \frac{TM5 - TM7}{TM5 + TM7} \quad (3)$$

where TM5 and TM7 denote Landsat TM bands 5 (1,550–1,750 nm) and 7 (2,080–2,350 nm), respectively [48]. Where equivalent Landsat TM data are unavailable, but ASTER data are, we calculate NDTI by replacing Landsat TM band 5 with ASTER band 4 and Landsat TM band 7 with the average value of ASTER bands 5–8. Hyperspectral reflectance data were convolved over the ASTER and Landsat TM band passes using sensor relative spectral response functions [45] to determine the equivalent bands for SINDRI, LCA, and NDTI.

### 3. Spectral Data Acquisition and Processing Methods

#### 3.1. Ground-Based Spectrophotometric Measurements

Ground-based measurements were acquired on several dates in 2002, 2003, and 2004 (data from Daughtry and Hunt [30]) over a number of corn, soybean, and wheat production fields in Beltsville, MD (Table 1) using an Analytical Spectral Devices Inc. Fieldspec Pro FR spectroradiometer (Boulder, CO) and calibrated using a 45 cm square Spectralon panel (Labsphere, Inc., North Sutton, NH). The spectrophotometer acquired 2,151 data points interpolated to 1-nm resolution between 350 and 2,500 nm. The crop residues had been present in the fields for approximately seven months. Ground measurements were acquired under varying soil and residue moisture and green cover conditions (Table 1). Bare soil, residue, and green vegetation were determined by classifying digital photographs acquired at nadir from a height of 2.3 m. Within these data sets, data points with a green vegetation cover of over 30% were excluded from analysis. Soil and crop residue water contents were determined gravimetrically by drying soils at 105 °C for 48 hours and crop residues 70 °C for four days. For more information on this specific data set, the reader is encouraged to refer to Daughtry and Hunt [30]. Reflectance spectra of green corn canopies were acquired in corn fields on 7 July 2006 at the silking (R1) stage for the corn [46] using the ASD spectroradiometer and the 18° fore-optic. Results from these spectra are shown in Figure 2.

#### 3.2. Air- and Space-Borne Measurements

Airborne hyperspectral data were acquired on several dates in the spring of 2006 and 2007 in Indiana, Illinois, Iowa, and Centreville, Maryland, by SpecTIR LLC (Sparks, NV, USA) as seen in Table 1. Airborne hyperspectral data acquired in 2006 consisted of 356 data points between 398.5 nm and 2,455.0 nm with a spectral resolution of approximately 4.8 nm between 398.5 nm and 953.5 nm and 6.3 nm between 964.1 nm and 2,455.0 nm. The airborne hyperspectral data from 2007 contained 178 data points between 400 and 2,450 nm with a spectral resolution of approximately 9.5 nm

between 400.7 nm and 951.0 nm and 12.6 nm between 967.2 nm and 2,451.8 nm. Spaceborne ASTER data were acquired on 22 May 2005 and 19 May 2007 for the Ames, IA area. All aircraft data had pixel sizes of 4 m with the exception of the Centreville, MD set, which were acquired at 2 m resolution. For aircraft data, atmospherically corrected reflectance data were further corrected for cross-track illumination effects, geometrically corrected, and mosaicked. Atmospherically and geometrically corrected surface reflectance ASTER imagery were acquired from the USGS EROS Data Center (Sioux Falls, SD) for the Ames, IA area with a pixel size of 30 m. Ground truth data were acquired using the line-point-transect method and located using a Garmin e-Trex handheld global positioning system (GPS) with 15-m field accuracy.

At a number of these locations soil and crop residue samples were also acquired for laboratory analysis. These soil and residue samples were then analyzed in the lab using the ASD spectrophotometer. Lab samples were illuminated by six 100-W quartz-halogen lamps mounted on the arms of a camera copy stand at 45 cm over the sample at a 45° illumination zenith angle. A current-regulated DC power supply stabilized the output of the lamps. A digital camera and the fore-optic of the spectroradiometer were aligned and positioned 90 cm from the sample surface at a 0° view zenith angle. A 1 fore-optic with a 1.6-cm-diameter field of view was used for the additional soil samples; an 18° fore-optic with a 28.5-cm-diameter field of view was used for the crop residues. The illumination and view angles were chosen to minimize shadowing and to emphasize the fundamental spectral properties of the samples.

Four spectra of 100 scans each were acquired from each sample by rotating the sample tray 90° after each spectrum. All samples were placed in trays that were spray painted flat black. A 61-cm square Spectralon reference panel was placed in the field of view, illuminated, and measured in the same manner as the samples. Reflectance factors were calculated and corrected for the reflectance of the Spectralon. Because the additional soil sample spectra were acquired using a different method than used by Brown *et al.* [18], the two data sets were analyzed separately, which included estimation of total soil carbon using a LECO TruSpec CN gas analyzer (LECO Corp., St. Joseph, MI) and soil carbonate content via modified pressure calcimetry [49]. Soil organic carbon contents were determined by subtracting the carbonate contents from the total carbon contents. In this work we only report ranges of values for the Iowa and Indiana sites.

Thirty-meter buffers were used around each GPS point to extract mean spectral signatures from imagery, with the exception of the Maryland imagery, where 20-m buffers were used due to the smaller field sizes. In all cases crop residues were present in the field at least seven months; soybean residues frequently contained corn residues from the previous year. Because green covers were not assessed with the hyperspectral and ASTER imagery, all data points were used.

### 3.3. Data Processing and ASTER Index Determination

The hyperspectral data acquired from the ASD spectrophotometer and the 2006 airborne hyperspectral data acquired in Indiana and Illinois were convolved to 178 data points using cubic spline interpolation, for comparative analysis with later airborne hyperspectral acquisitions in Iowa, Indiana, and Maryland. These data were then used to compute three-dimensional generalized normalized difference index (gNDI) matrices via:

$$gNDI_{i,j,k} = \frac{R_{i,k} - R_{j,k}}{R_{i,k} + R_{j,k}} \quad (4)$$

where  $R$  denotes reflectance and the subscripts  $i$  and  $j$  denote wavelengths for sampling location  $k$ . The coefficients of determination ( $r^2$ ) were calculated for each  $gNDI_{ij}$  set against line-point transect measured  $f_R$  for assessment of correlation. Lastly, a composite  $gNDI$   $r^2$  value was determined by averaging the  $gNDI$   $r^2$  values for all of the hyperspectral data sets.

Additionally, all hyperspectral data were convolved to the nine ASTER visible, near-infrared, and SWIR bands and to equivalent Landsat TM 5 bands utilizing their relative spectral response functions [45]. Like with the hyperspectral data, Equation (4) was utilized and the data analyzed in a similar manner. These data were also used to calculate spectral indices using Equations (1–3).

Pixels with green vegetation were excluded using the Normalized Difference Vegetation Index (NDVI) [50]:

$$NDVI = \frac{NIR - Red}{NIR + Red} \quad (5)$$

where  $NDVI > 0.3$  was assumed for green vegetation pixels with  $Red$  and  $NIR$  being ASTER bands 2 (630–690 nm) and 3 (760–860 nm), respectively [47].

The relationships between  $f_R$  and selected spectral indices were performed utilizing linear regression, with  $r^2$  calculated to determine goodness-of-fit. Regression line slope and intercept values were used to calculate remote estimates of  $f_R$ , which in turn were compared with ground-truth  $f_R$  estimates. Root-mean-square error (RMSE) values were calculated between ground-truth and remote estimates of  $f_R$ . Additionally,  $3 \times 3$  tillage classification accuracy parameters were assessed, including  $Z$ -statistic (which tests the null hypothesis that the classification accuracy is not significantly different from random chance) and  $k$ -hat (estimate of the kappa statistic) values [51]. The tillage classes are defined as intensive tillage having  $f_R < 0.15$ , reduced tillage with  $0.15 \leq f_R < 0.3$ , and conservation tillage (no-till, ridge-till, and mulch-till) at  $f_R > 0.3$  as defined by the USDA-NRCS and the Conservation Technology Information Center [52] for operational purposes. Classifications are considered significant at the 95% confidence level if the  $Z$ -statistic  $> 1.96$  [51].

The air- and spaceborne imagery were classified to live vegetation and three  $f_R$  classes utilizing the decision tree classifier in ENVI (ITT Visual Solutions, Boulder, CO). All classified images were then subjected to a  $5 \times 5$  majority analysis to minimize noise.

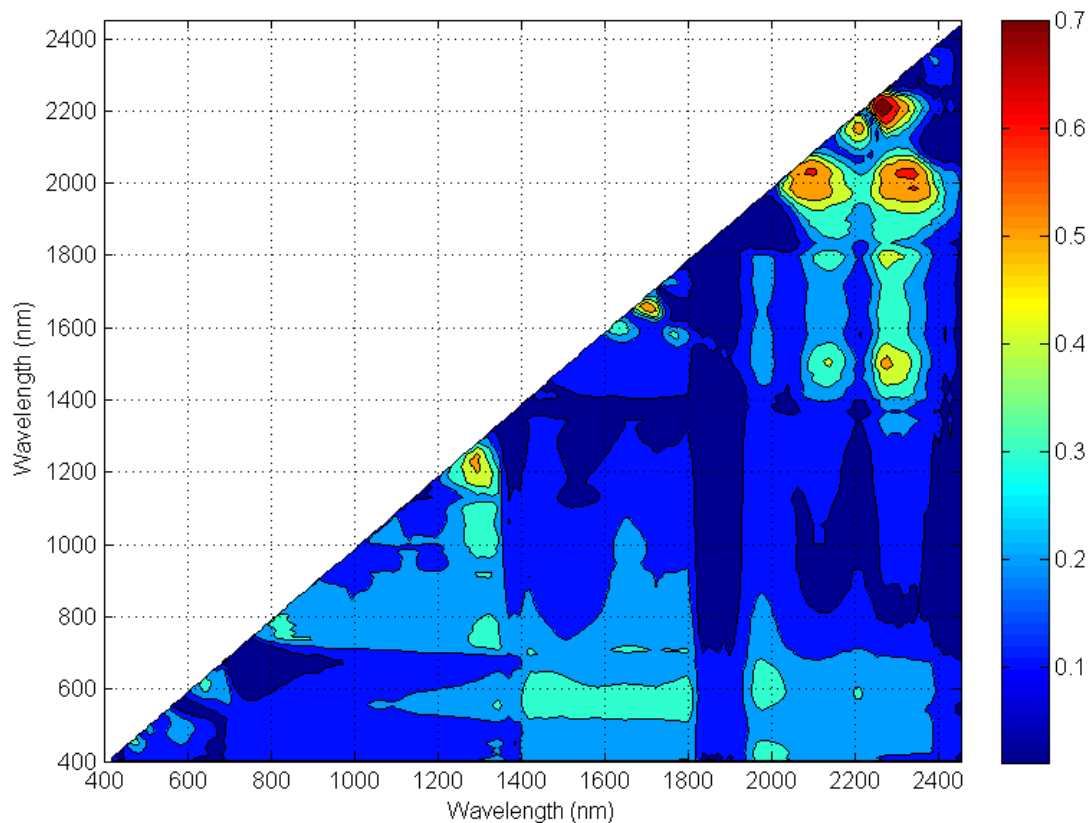
## 4. Results and Discussion

### 4.1. Hyperspectral and ASTER Index Determination

Comparison of composite  $r^2$  values for  $gNDI_{ij}$  against  $f_R$  showed the best correlation occurring for the wavelength pair at 2,210 and 2,260 nm (Figure 3), with  $r^2 = 0.759$ . Hence, the hyperspectral Shortwave Infrared Normalized Difference Residue Index (hSINDRI) is defined as:

$$hSINDRI = \frac{R_{2210} - R_{2260}}{R_{2210} + R_{2260}} \quad (6)$$

**Figure 3.** Composite coefficient of determination ( $r^2$ ) values for all data sets mentioned in Table 1 for general normalized difference indices (gNDI<sub>*i,j*</sub>) in comparison with line-point transect crop residue cover ( $f_R$ ) estimates.



Since  $R_{2210}$  and  $R_{2260}$  correspond with ASTER bands 6 (2,185–2,225 nm) and 7 (2,235–2,285 nm) [47], the ASTER Shortwave Infrared Normalized Difference Residue Index (SINDRI) is defined as:

$$SINDRI = \frac{ASTER6 - ASTER7}{ASTER6 + ASTER7} \quad (7)$$

where ASTER6 and ASTER7 denote ASTER SWIR bands 6 and 7, respectively. In addition to the hyperspectral gNDI<sub>*i,j*</sub> analysis, and ASTER gNDI<sub>*i,j*</sub> analysis was conducted to affirm the validity of SINDRI. Comparison of all 36 possible pairwise ASTER band combinations as normalized differences showed the best residue index indeed used ASTER bands 6 and 7, with a composite  $r^2$  value for all data sets of 0.741 (Table 2).

**Table 2.** Composite coefficient of determination ( $r^2$ ) values for all pairwise combinations of normalized difference indices ( $gNDI_{i,j}$ ) compared with ground truth crop residue cover ( $f_R$ ) estimates for the NASA Terra Advanced Spaceborne Thermal Emission and Reflection Radiometer (ASTER) sensor bands. The  $gNDI_{i,j}$  band combination which correlates the best for all data sets in Table 1 is highlighted in bold and italicized. FWHM denotes full-width-half-maximum wavelength bands [47].

FWHM bandwidth (nm)	520–600	630–690	760–860	1600–1700	2145–2185	2185–2225	2235–2285	2295–2365	2360–2430
ASTER band	1	2	3	4	5	6	7	8	9
1	-								
2	0.173	-							
3	0.101	0.104	-						
4	0.298	0.257	0.239	-					
5	0.287	0.267	0.150	0.270	-				
6	0.289	0.273	0.159	0.206	0.495	-			
7	0.284	0.267	0.149	0.362	0.557	<b><i>0.741</i></b>	-		
8	0.269	0.266	0.154	0.342	0.298	0.456	0.140	-	
9	0.240	0.243	0.136	0.206	0.096	0.171	0.091	0.175	-

Composite values of  $r^2$  and RMSE from all test locations (Table 1) show SINDRI performing better than LCA and NDTI, but not as well as CAI. Comparison of index values from Beltsville, MD (Figure 4), Fulton, IN (Figure 5), Ames, IA (Figure 6), and Pesotum, IL and Centreville, MD (Figure 7) show that CAI and SINDRI values are relatively close to the regression line. LCA values show larger relative deviations of values from the regression line than do CAI or SINDRI. The largest deviations occurred with NDTI. The slope and deviation of index values were dependent also on location, sensor, and acquisition date. Data from Beltsville, MD (Figure 4) show that NDTI was the most affected by acquisition date, with the data set from 10 June 2003 having a regression line slope that is almost perpendicular to the other dates; SINDRI on the other hand shows the least deviation in the slope line from the other dates and usually had parallel regression lines. Similar behavior with NDTI can be seen for both the Indiana (Figure 5) and Iowa (Figure 6) data sets, whereby the latest growing season dates have the lowest regression line slopes. This change in slope is likely attributable to two factors. Firstly, the increased presence of green vegetation in the field (Figure 8) greatly affects NDTI [17]. Secondly, there were the radiometric differences between the aircraft hyperspectral and ASTER sensors, including atmospheric effects (including the sensor altitude above the target area). Convolved ASTER NDTI was compared with convolved equivalent Landsat TM NDTI for the 27 May 2007 Ames, IA data set in Figure 9, where the two sets of values lined up and were close to the 1:1 line. Aircraft and ASTER derived SINDRI values showed distinct offsets in values between the two sensor types, with the aircraft-derived data (27 May 2007 in Figure 6) showing higher index values than the two ASTER-derived data sets, which had overlapping values.

**Figure 4.** Comparison of crop residue cover ( $f_R$ ) and  $f_R$  index values with regression lines for the Beltsville, MD data sets [30]. Index acronyms: CAI–Cellulose Absorption Index; SINDRI–Shortwave Infrared Normalized Difference Residue Index; LCA–Lignin-Cellulose Absorption Index; and NDTI–Normalized Difference Tillage Index. Straight lines denote regression lines. Dotted lines denote tillage class boundaries. Data were acquired with an ASD Inc. Fieldspec Pro FR spectroradiometer (Boulder, CO).

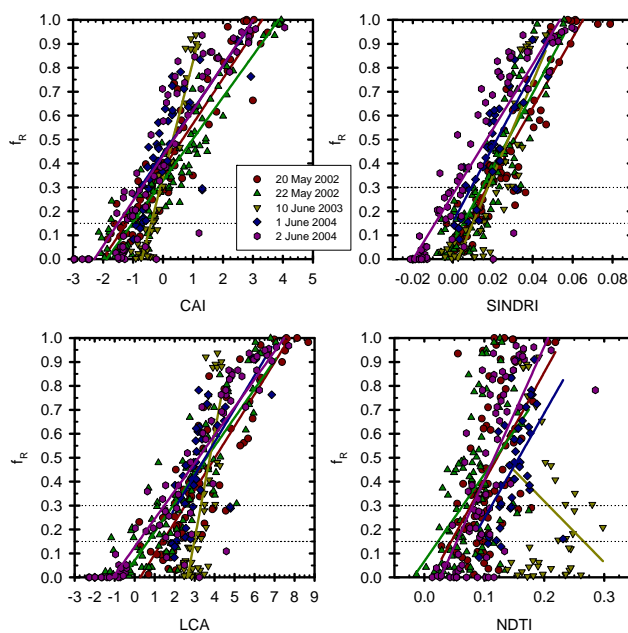


**Figure 5.** Comparison of crop residue cover ( $f_R$ ) and  $f_R$  index values with regression lines for Fulton, IN, 29 May 2006. Index acronyms: CAI – Cellulose Absorption Index; SINDRI–Shortwave Infrared Normalized Difference Residue Index; LCA–Lignin-Cellulose Absorption Index; and NDTI–Normalized Difference Tillage Index. Straight lines denote regression lines. Dotted lines denote tillage class boundaries. Data were acquired from aircraft by SpectTIR LLC (Sparks, NV).

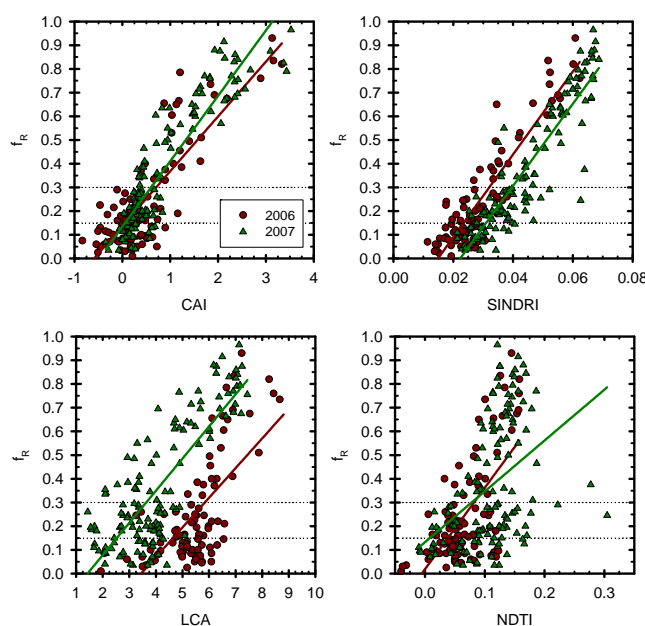
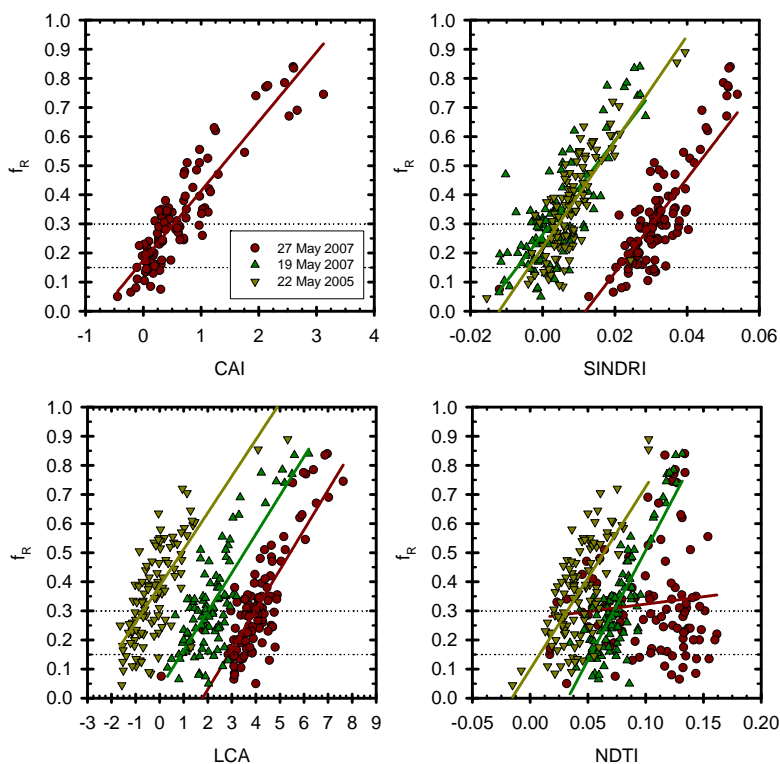


**Figure 6.** Comparison of crop residue cover ( $f_R$ ) and  $f_R$  index values with regression lines for the Ames, IA area. Index acronyms: CAI–Cellulose Absorption Index; SINDRI–Shortwave Infrared Normalized Difference Residue Index; LCA–Lignin-Cellulose Absorption Index; and NDTI–Normalized Difference Tillage Index. Straight lines denote regression lines. Dotted lines denote tillage class boundaries. 22 May 2005 and 19 May 2007 multispectral data were acquired by the ASTER sensor. 27 May 2007 hyperspectral data were acquired from aircraft by SpectIR LLC (Sparks, NV). CAI is only available for 27 May 2007 imagery.



When assessing the classification accuracy [51] with the three tillage classes, composite SINDRI values fared similarly to CAI, and much better than LCA and NDTI (Table 1). Classifications using the four indices from the 2006 Fulton, IN show the best visual agreement for CAI and SINDRI with ground-truth; LCA and NDTI did not fare as well (Figure 10). For all data sets in Table 1 SINDRI classifications were significantly better than random at a 95% confidence level; CAI and LCA yielded significant classifications except for the Beltsville, MD data set on 1 June 2004, and NDTI classifications failed significance tests for six of the thirteen data sets.

**Figure 7.** Comparison of crop residue cover ( $f_R$ ) and  $f_R$  index values with regression lines for the Pesotum, IL (PIL) and Centreville, MD (CMD) areas. Index acronyms: CAI–Cellulose Absorption Index; SINDRI–Shortwave Infrared Normalized Difference Residue Index; LCA–Lignin-Cellulose Absorption Index; and NDTI–Normalized Difference Tillage Index. Straight lines denote regression lines. Dotted lines denote tillage class boundaries. Data were acquired from aircraft by SpecTIR LLC (Sparks, NV).

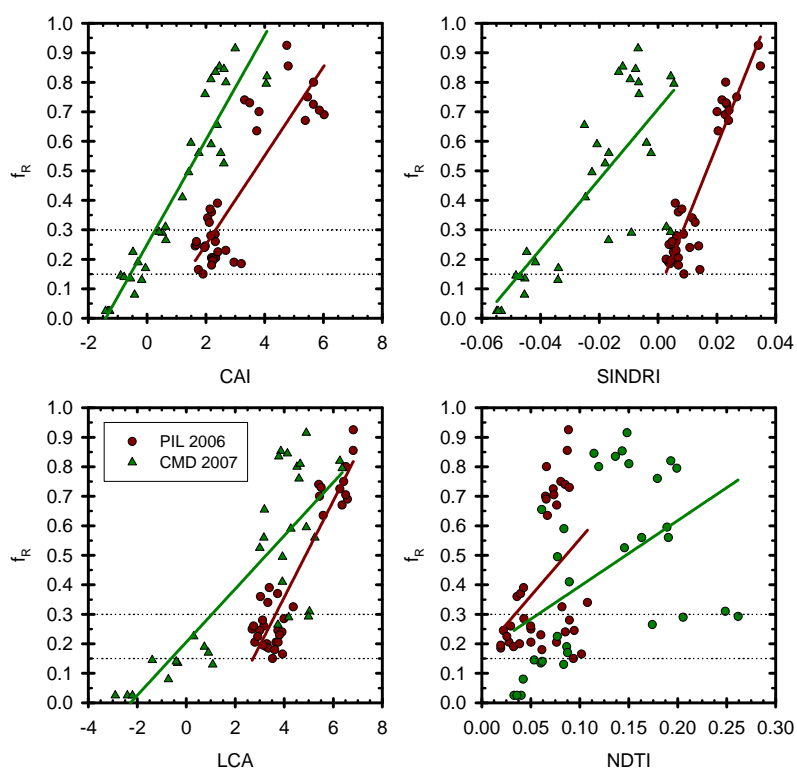


**Figure 8.** Range of ASTER derived NDVI values for each data set. BMD, CMD, AIA, FIN, and PIL denote data from the Beltsville, MD, Centreville, MD, Ames, IA, Fulton, IN, and Pesotum, IL sites, respectively. Black dots denote outlier values above the 10th and below and the 90th percentile values (whiskers), the box denotes values between the 25th and 75th percentiles, with the median values being the bars in the middle of the boxes.

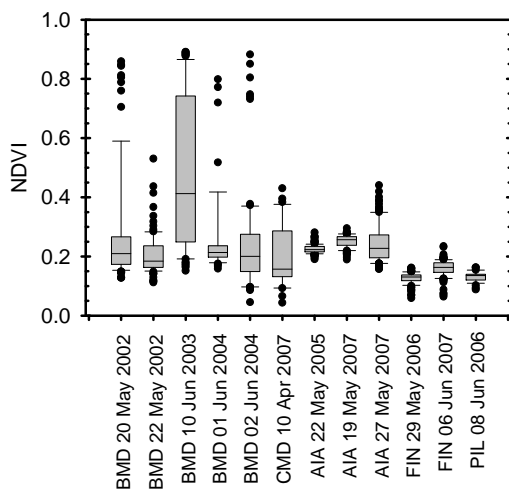


**Figure 9.** Comparison of ASTER and Landsat TM NDTI values for the Ames, IA area on 27 May 2007.

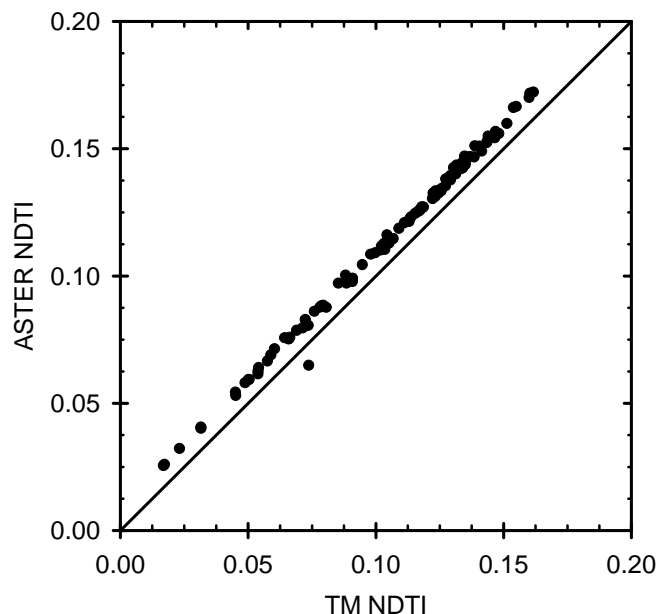
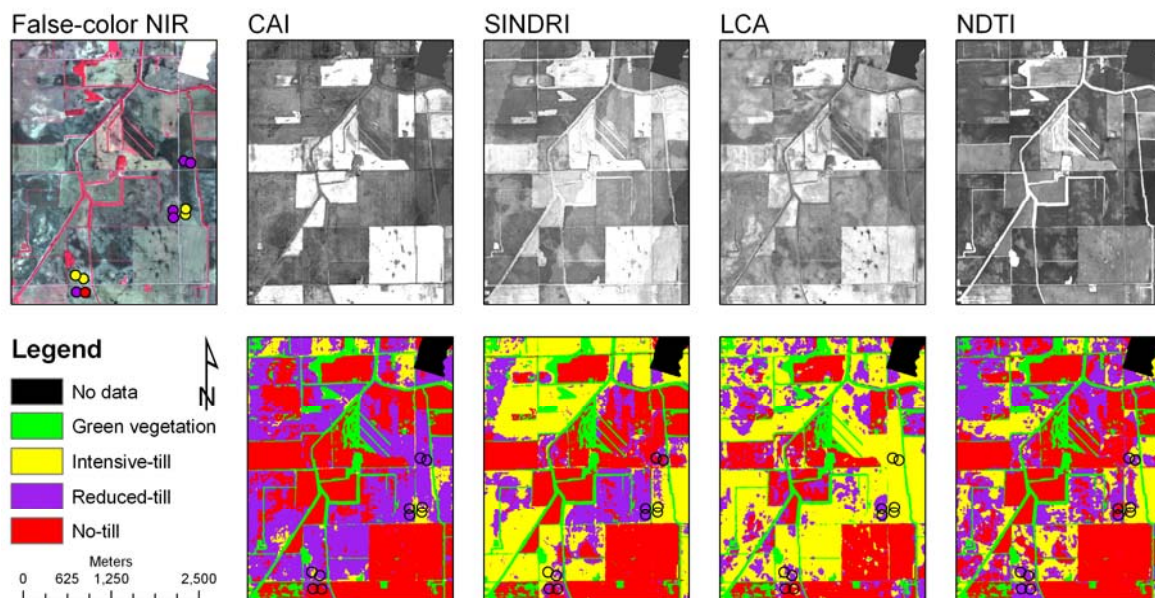


**Figure 10.** Comparison of crop residue indices and classification results for Fulton, IN, 29 May 2006. The false-color NIR image utilized narrow spectral bands (red–860.7 nm, green–648.2 nm, and blue–548.2 nm) and is shown to help the reader differentiate between green vegetation pixels and non-vegetated fields that were undergoing tillage and planting operations. CAI is calculated from hyperspectral data, and the other indices via hyperspectral data that were convolved to equivalent ASTER (SINDRI and LCA) and Landsat TM (NDTI) bands. Classification results were post processed using a  $5 \times 5$  majority analysis to minimize noise. Circles denote ground-truth locations. Color-coded circles in the false-color NIR image denote ground truth tillage classes. Data were acquired from aircraft by SpecTIR LLC (Sparks, NV).

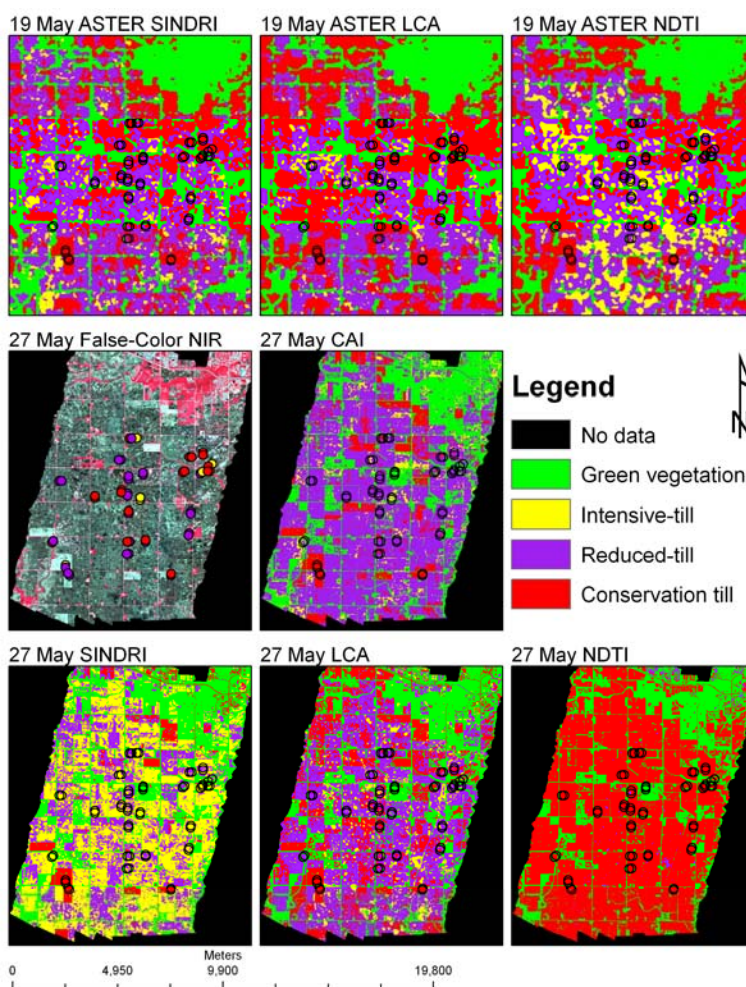


NDTI seemed to be the most affected by soil spectral properties, specifically soil carbon, as denoted by dark areas in the false color-NIR image in Figure 10. In the Fulton, IN area soil carbon was found to range between 0.5%–44.9% on a mass basis, with higher SOC soils being darker than low-SOC soils [17,34]. SINDRI was found to be sensitive to green vegetation, whereby pixels with high normalized difference vegetation index (NDVI) also had high values of SINDRI, unlike CAI for which green vegetation had values around zero [17,43]. However, pixels with NDVI above a specific value (for this study 0.3) can be masked out during image processing. NDTI also appeared to work the best when calculated from ASTER bands. However, ASTER NDTI values were only calculated for Iowa, and this may be a function of date within the season as seen with the regression line slopes in Figures 4–6. Iowa May 2007 NDTI statistical parameters decreased greatly between the ASTER acquisition on May 19 and the airborne hyperspectral acquisition in May 27 (Tables 1 and 3, and Figure 11), with only the 19 May 2007 NDTI classification being significantly different from random (Table 1). SINDRI showed comparable results to CAI, except in green vegetation pixels, but these were excluded from the analysis by the use of NDVI. Figure 11 shows classification maps for the imagery acquired southwest of Ames, IA. In this area the range of SOC values was less than for the Indiana site and ranged between 0.5% and 6.5%. Spectral indices for ASTER imagery acquired on 19 May 2007 show that most non-vegetated field pixels are classified as either reduced or conservation tillage (Table 3), with statistical parameters being similar for all indices, albeit that for this data set ASTER NDTI performed the best. For the 27 May 2007 data set shown in Figure 11 and Table 3, CAI classified most fields as being reduced-till, and airborne SINDRI as intensive till. Airborne LCA visually agreed the best with CAI. Airborne NDTI did not produce a significant classification (Table 1) due to the nearly flat regression line for the data in Figure 6. However, for the 27 May 2007 data SINDRI performed the best with respect to classification accuracy, although CAI had a higher  $r^2$  and lower RMSE when comparing ground-truth and remote estimates of  $f_R$ . It should be noted that 2007 ground-truth acquisition activities in Iowa occurred on May 21–23, so there was a distinct possibility that changes in tillage occurred between the ASTER image acquisition on May 19 and the airborne hyperspectral image acquisition on May 27. This is further evidenced in Figure 11 and Table 3, where both SINDRI and LCA show shifts toward lower-  $f_R$  classes between the two dates. Additionally, a heavy rain event of 8.46 cm (3.33 inches) was reported on May 24 with 0.66 cm (0.26 inches) more rain being reported on May 26 by the National Weather Service for Ames, IA [53]. This rain could have hampered any ongoing tillage and planting operations. The rain could also have encouraged plant canopy growth, and coupled with the previous day's the rain increased total scene water, adversely affecting TM bands 5 and 7 [54], and thus, NDTI, while minimally impacting the other indices. Unfortunately, no water content measurements of crop residue or surface soil were acquired on the days of acquisition; however, the maximum NDVI values did increase between those two dates (Figure 8).

**Table 3.** Tillage class areas and percents as determined by spectral index classifications and following a 5 × 5 majority analysis for the images southwest of Ames, IA in 2007 as displayed in Figure 11. 19 May 2007 imagery included an average non-vegetated field area of 10928.6 ha southwest of Ames, IA, and 27 May 2007 imagery averaged 7792.8 ha. Green vegetation pixels were excluded from the analysis. Conserv. denotes conservation tillage.

Tillage class	19 May 2007						27 May 2007							
	SINDRI		LCA		NDTI		CAI		SINDRI		LCA		NDTI	
	Area (ha)	%	Area (ha)	%	Area (ha)	%	Area (ha)	%	Area (ha)	%	Area (ha)	%	Area (ha)	%
Intensive	843.8	7.9	443.9	4.1	1681.7	14.9	577.9	7.5	4285.6	55.3	660.6	8.5	0.0	0.0
Reduced	5941.5	55.5	4610.0	42.6	5280.1	46.8	6064.3	78.2	2819.9	36.4	4643.3	59.8	133.9	1.7
Conserv.	3918.2	36.6	5755.8	53.2	4310.8	38.2	1110.4	14.3	638.0	8.2	2461.8	31.7	7735.2	98.3

**Figure 11.** Comparison of crop residue indices and classification results for the area southwest of Ames, IA. The top three images were calculated from 19 May 2007 multispectral ASTER imagery; the bottom five are derived from airborne hyperspectral imagery acquired by SpectTIR LLC (Sparks, NV) on 27 May 2007. 27 May SINDRI, LCA, and NDTI were calculated from convolved equivalent ASTER and Landsat TM bands. Circles denote ground-truth locations. Color-coded circles in the 27 May 2007 false-color NIR image denote ground truth tillage classes.



It should be noted, however, that care needs to be taken when assessing the quality of indices and classifications based upon regression, RMSE, and classification accuracy analyses [51]. This is particularly the case, as the  $f_R$ -based tillage classification scheme utilized by the USDA-NRCS and the CTIC [52], utilizes relatively narrow  $f_R$  classes for intensive-(0%–15%) and reduced-tillage (15%–30%), and a much wider third cover class, conservation tillage (30%–100%). This, in conjunction with inherent difficulties in the line-point transect and digital photographic methods that were used for ground-truth acquisition [10,55] and changes in  $f_R$  over very small distances (i.e., within the sampling area), can easily create a situation where remote and ground truth  $f_R$   $r^2$  and RMSE values may be slightly inconsistent with classification accuracy parameters in comparison with another data set, particularly when data points occur near class boundaries.

#### 4.2. Effect of Water Content on Index Value

High soil water content values reported for the Beltsville, MD samples by Daughtry and Hunt [30] decreased  $r^2$  and increased RMSE values (Table 1) for SINDRI, suggesting this index may be problematic soon after irrigation or precipitation.  $3 \times 3$  accuracy assessments were similarly negatively affected by increase in water content, but consistently produced significant classifications even in the one case where CAI and LCA did not on 1 June 2004 (Table 1). Furthermore, SINDRI did performed well in Iowa in the days after a heavy rain event, with another occurring the day prior to acquisition. Thus, SINDRI appears to be robust even in somewhat wet conditions. However, we feel that additional research is needed to fully assess the effects of water content on SINDRI.

### Conclusions

SINDRI effectively estimated  $f_R$  at multiple locations on several dates. SINDRI also tracked changes in tillage for the same location in two images that were acquired eight days apart. While CAI still performed the best, SINDRI performed better than both LCA and NDTI. NDTI was the most inconsistent index in terms of accuracy and produced insignificant classifications for six of the thirteen data sets analyzed. SINDRI offers a viable option for  $f_R$  mapping at less cost compared to CAI. SINDRI also allows for reanalysis of existing ASTER imagery for crop residue and other non-photosynthetic vegetation cover. These data, in turn, can be used as input parameters for agricultural carbon and erosion models that are dependent upon tillage and  $f_R$  data. As such, this index would also be useful for monitoring carbon sequestration to reduce the rate of increase in atmospheric CO<sub>2</sub> concentrations.

SINDRI was found to be somewhat sensitive to green vegetation and soil and crop residue water content, but still produced robust results in wet conditions. However, accurate results can still be acquired even with these present. Green vegetation pixels should be masked out utilizing a vegetation index such as NDVI prior to analysis with SINDRI.

Further research is needed to assess (a) SINDRI's applicability over a wider range of geographic areas, (b) the sensitivity of SINDRI to water content, and (c) to assess its usefulness for other applications where detection of non-photosynthetic vegetation is of interest, e.g., rangeland health or brush fire hazards.

## Acknowledgements

We gratefully acknowledge Adam Hidey, Michael Bayless, Lawrence Corp, Alan Stern, Adam Booher, Charissa Luman, and Andrew Russ for their assistance in field work and data processing. Wade Crow is acknowledged for his assistance in manuscript preparation.

## References and Notes

1. Causarano, H.J.; Doraiswamy, P.C.; McCarty, G.W.; Hatfield, J.L.; Milak, S.; Stern, A.J. EPIC modeling of soil organic carbon sequestration in croplands of Iowa. *J. Environ. Qual.* **2008**, *37*, 1345-1353.
2. Causarano, H.J.; Franzluebbers, A.J.; Reeves, D.W.; Shaw, J.N. Soil organic carbon sequestration in cotton production systems of the southeastern United States: A review. *J. Environ. Qual.* **2006**, *35*, 1374-1383.
3. Monfreda, C.; Ramankutty, N.; Foley, J.A. Farming the planet: 2. Geographic distribution of crop areas, yields, physiological types, and net primary production in the year 2000. *Global Biogeochem. Cycle* **2008**, *22*, 1-19.
4. Ramankutty, N.; Evan, A.T.; Monfreda, C.; Foley, J.A. Farming the planet: 1. Geographic distribution of global agricultural lands in the year 2000. *Global Biogeochem. Cycle* **2008**, *22*, GB1003.
5. Archer, D.W.; Halvorson, A.D.; Reule, C.A. Economics of irrigated continuous corn under Conventional-Till and No-Till in Northern Colorado. *Agron. J.* **2008**, *100*, 1166-1172.
6. Paudel, K.P.; Lohr, L.; Cabrera, M., Residue management systems and their implications for production efficiency. *Renew. Agr. Food Syst.* **2006**, *21*, 124-133.
7. McGinnis, L. Show me the money: Why economics is essential for sustainable agriculture. *Agr. Res.* **2007**, *55*, 8-11.
8. Lal, R. World crop residues production and implications of its use as a biofuel. *Environ. Int.* **2005**, *31*, 575-584.
9. Laflen, J.M.; Amemiya, M.; Hintz, E.A. Measuring crop residue cover. *J. Soil Water Conserv.* **1981**, *36*, 341-343.
10. Morrison, J.E., Jr.; Huang, C.H.; Lightle, D.T.; Daughtry, C.S.T. Residue measurement techniques. *J. Soil Water Conserv.* **1993**, *48*, 479-483.
11. Daughtry, C.S.T. Discriminating crop residues from soil by shortwave infrared reflectance. *Agron. J.* **2001**, *93*, 125-131.
12. Daughtry, C.S.T.; Hunt, E.R., Jr.; Doraiswamy, P.C.; McMurtrey, J.E., III. Remote sensing the spatial distribution of crop residues. *Agron. J.* **2005**, *97*, 864-871.
13. McNairn, H.; Protz, R. Mapping corn residue cover on agricultural fields in Oxford County, Ontario, using Thematic Mapper. *Can. J. Remote Sens.* **1993**, *19*, 152:159.
14. van Deventer, A.P.; Ward, A.P.; Gowda, P.H.; Lyon, J.G. Using Thematic Mapper data to identify contrasting soil plains to tillage practices. *Photogramm. Eng. Remote Sens.* **1997**, *63*, 87-93.

15. Qi, J.; Marsett, R.; Heilman, P.; Biedenbender, S.; Moran, S.; Goodrich, D.; Weltz, M. RANGES improves satellite-based information and land cover assessments in southwest United States. *Eos* **2002**, *83*, 601-606.
16. Biard, F.; Baret, F. Crop residue estimation using multiband reflectance. *Remote Sens. Environ.* **1997**, *59*, 530-536.
17. Serbin, G.; Daughtry, C.S.T.; Hunt, E.R., Jr.; Brown, D.J.; McCarty, G.W. Effect of soil spectral properties on remote sensing of crop residue cover. *Soil Sci. Soc. Am. J.* **2009**, *73*, 1545-1558.
18. Brown, D.J.; Shepherd, K.D.; Walsh, M.G.; Mays, M.D.; Reinsch, T.G. Global soil characterization with VNIR diffuse reflectance spectroscopy. *Geoderma* **2006**, *132*, 273-290.
19. U. S. Geological Survey USGS EO-1 Website; Available online: <http://eo1.usgs.gov/hyperion.php> (accessed 25 August 2009).
20. Gill, T.K.; Phinn, S.R. Estimates of bare ground and vegetation cover from Advanced Spaceborne Thermal Emission and Reflection Radiometer (ASTER) short-wave-infrared reflectance imagery. *J. Appl. Remote Sens.* **2008**, *2*, 023511.
21. Gill, T.K.; Phinn, S.R. Improvements to ASTER-derived fractional estimates of bare ground in a savanna rangeland. *IEEE Trans. Geosci. Remote Sens.* **2009**, *47*, 662-670.
22. Chikhaoui, M.; Bonn, F.; Bokoye, A.I.; Merzouk, A. A spectral index for land degradation mapping using ASTER data: Application to a semi-arid Mediterranean catchment. *Int. J. Appl. Earth Obs. Geoinformation* **2005**, *7*, 140-153.
23. Lewis, D.; Yao, H.; Fridgen, J.; Kincaid, R. Investigation on the Potential of using ASTER Image for Corn Plant Residue Coverage Estimation in Three Indiana Counties, 2006 *IEEE International Geoscience & Remote Sensing Symposium IGARSS'06*. IEEE Geoscience and Remote Sensing Society: Denver, CO, USA, 2006; pp. 2092-2094.
24. NASA Jet Propulsion Laboratory SWIR—ASTER User Advisory; Available online: <http://asterweb.jpl.nasa.gov/swir-alert.asp> (accessed 7 July, 2009).
25. Baumgardner, M.F.; Silva, L.F.; Biehl, L.L.; Stoner, E.R. Reflectance properties of soils. In *Advances in Agronomy*. Volume 38; Brady, N.C., Ed.; Academic Press, Inc.: New York, NY, USA, 1985; pp. 2-44.
26. Clark, R.N. Spectroscopy of rocks and minerals, and principles of spectroscopy. In *Manual of Remote Sensing, Volume 3, Remote Sensing for the Earth Sciences*, Rencz, A.N., Ed. John Wiley and Sons: New York, NY, USA, 1999; pp 3-58.
27. Clark, R.N.; Swayze, G.A.; Livo, K.E.; Kokaly, R.F.; Sutley, S.J.; Dalton, J.B.; McDougal, R.R.; Gent, C.A. Imaging spectroscopy: Earth and planetary remote sensing with the USGS Tetracorder and expert systems. *J. Geophys. Res. Planets* **2003**, *108*, 5131, doi:10.1029/2002JE001847.
28. Stoner, E.R.; Baumgardner, M.F. Characteristic variations in reflectance of surface soils. *Soil Sci. Soc. Am. J.* **1981**, *45*, 1161-1165.
29. Waiser, T.H.; Morgan, C.L.S.; Brown, D.J.; Hallmark, C.T. In situ characterization of soil clay content with visible near-infrared diffuse reflectance spectroscopy. *Soil Sci. Soc. Am. J.* **2007**, *71*, 389-396.
30. Daughtry, C.S.T.; Hunt, E.R., Jr. Mitigating the effects of soil and residue water contents on remotely sensed estimates of crop residue cover. *Remote Sens. Environ.* **2008**, *112*, 1647-1657.

31. Lobell, D.B.; Asner, G.P. Moisture effects on soil reflectance. *Soil Sci. Soc. Am. J.* **2002**, *66*, 722-727.
32. Nagler, P.L.; Daughtry, C.S.T.; Goward, S.N. Plant litter and soil reflectance. *Remote Sens. Environ.* **2000**, *71*, 207-215.
33. Whiting, M.L.; Li, L.; Ustin, S.L. Predicting water content using Gaussian model on soil spectra. *Remote Sens. Environ.* **2004**, *89*, 535-552.
34. Serbin, G.; Daughtry, C.S.T.; Hunt, E.R., Jr.; McCarty, G.W.; Doraiswamy, P.C.; Brown, D.J. Improved remotely-sensed estimates of crop residue cover by incorporating soils information. In *2008 IEEE International Geoscience & Remote Sensing Symposium IGARSS'08*, IEEE Geoscience and Remote Sensing Society: Boston, MA, USA, 2008.
35. Salisbury, J.W.; Hunt, G.R. Martian surface materials: effect of particle size on spectral behavior. *Science* **1968**, *161*, 365-366.
36. Ben-Dor, E.; Goldshleger, N.; Benyamini, Y.; Agassi, M.; Blumberg, D.G. The spectral properties of soil structural crusts in the 1.2- to 2.5- $\mu\text{m}$  spectral region. *Soil Sci. Soc. Am. J.* **2003**, *67*, 289-299.
37. Ben-Dor, E. Quantitative remote sensing of soil properties. In *Advances in Agronomy*. Volume 75; Sparks, D., Ed.; Academic Press: San Diego, CA, USA, 2002; pp. 173-244.
38. Ben-Dor, E.; Chabrillat, S.; Demattê, J.A.M.; Taylor, G.R.; Hill, J.; Whiting, M.L.; Sommer, S. Using Imaging Spectroscopy to study soil properties. *Remote Sens. Environ.* **2009**, *113*, S38-S55.
39. Green, R.O. Measuring the spectral expression of carbon dioxide in the solar reflected spectrum with AVIRIS. In *Tenth Annual JPL Airborne Earth Science Workshop*, California Institute of Technology Jet Propulsion Laboratory: Pasadena, CA, USA, 2001.
40. Workman, J., Jr.; Weyer, L. *Practical Guide to Interpretive Near-Infrared Spectroscopy*. Taylor & Francis Group: Boca Raton, FL, USA, 2008; p. 332.
41. Elvidge, C.D. Visible and near infrared reflectance characteristics of dry plant materials. *Int. J. Remote Sens.* **1990**, *11*, 1775-1795.
42. Kokaly, R.F.; Clark, R.N. Spectroscopic determination of leaf biochemistry using band-depth analysis of absorption features and stepwise multiple linear regression. *Remote Sens. Environ.* **1999**, *67*, 267-287.
43. Serbin, G.; Daughtry, C.S.T.; Hunt, E.R., Jr.; Reeves, J.B., III; Brown, D.J. Effects of soil composition and mineralogy on remote sensing of crop residue cover. *Remote Sens. Environ.* **2009**, *113*, 224-238.
44. Sabins, F.F., Jr. *Remote Sensing: Principles and Interpretation*. 2nd edition; W. H. Freeman and Company: New York, NY, USA, 1987; p 449.
45. U. S. Geological Survey Spectral Characteristics Viewer. [http://landsat.usgs.gov/tools\\_viewer.php](http://landsat.usgs.gov/tools_viewer.php) (accessed 7 August 2009).
46. Ritchie, S.W.; Hanway, J.J.; Benson, G.O. *How a Corn Plant Develops, Special Report No. 48*. Iowa State University of Science and Technology Cooperative Extension Service: Ames, IA, USA, 2005; p 21.
47. Yale University Center for Earth Observation ASTER; Available online: <http://www.yale.edu/ceo/Documentation/ASTER.pdf> (accessed 7 August 2009).

48. NASA Goddard Space Flight Center The Landsat Program; Available online: <http://landsat.gsfc.nasa.gov/> (accessed 16 August 2009).
49. Sherrod, L.A.; Dunn, G.; Peterson, G.A.; Kolberg, R.L. Inorganic carbon analysis by modified pressure-calorimeter method. *Soil Sci. Soc. Am. J.* **2002**, *66*, 299-305.
50. Rouse, J.W., Jr.; Haas, R.H.; Deering, D.W.; Schell, J.A. *Monitoring the vernal advancement and retrogradation (green wave effect) of natural vegetation*; Texas A&M University: College Station, TX, USA, 1973; p. 93.
51. Congalton, R.G.; Green, K. *Assessing the Accuracy of Remotely Sensed data: Principles and Practices*. 2nd Ed.; CRC Press: Boca Raton, FL, USA, 2009; p. 183.
52. Conservation Technology Information Center 2009 CTIC Crop Residue Management Survey System; Available online: <http://www.crmsurvey.org/> (accessed 12 August 2009).
53. National Weather Service. *Record of Evaporation and Climatological Observations Ames 8 WSW*; NOAA National Weather Service National Climatic Data Center: Silver Spring, MD, USA, May, 2007.
54. Hunt, E.R., Jr.; Rock, B.N. Detection of changes in leaf water content using near- and middle-infrared reflectances. *Remote Sens. Environ.* **1989**, *30*, 43-54.
55. Morrison, J.E.; Rickman, R.W.; McCool, D.K.; Pfeiffer, K.L. Measurement of wheat residue cover in the Great Plains and Pacific Northwest. *J. Soil Water Conserv.* **1997**, *52*, 59-65.

© 2009 by the authors; licensee Molecular Diversity Preservation International, Basel, Switzerland. This article is an open-access article distributed under the terms and conditions of the Creative Commons Attribution license (<http://creativecommons.org/licenses/by/3.0/>).